

# Results on Identified Hadrons from the PHENIX Experiment at RHIC

T. Chujo<sup>a</sup> for the PHENIX Collaboration\*

<sup>a</sup>Brookhaven National Laboratory, Upton, NY 11973-5000, USA

Recent results on identified hadrons from the PHENIX experiment in Au+Au collisions at mid-rapidity at  $\sqrt{s_{NN}} = 200$  GeV are presented. The centrality dependence of transverse momentum distributions and particle ratios for identified charged hadrons are studied. The transverse flow velocity and freeze-out temperature are extracted from  $p_T$  spectra within the framework of a hydrodynamic collective flow model. Two-particle HBT correlations for charged pions are measured in different centrality selections for a broad range of transverse momentum of the pair. Results on elliptic flow measurements with respect to the reaction plane for identified particles are also presented.

## 1. INTRODUCTION

The physics motivation of the ultra-relativistic heavy-ion program at the Relativistic Heavy Ion Collider (RHIC) is to study nuclear matter at extremely high temperature and energy density with the hope to reach a new form of matter called the quark gluon plasma (QGP). Among the various probes of the QGP state, hadrons carry important information about the collision dynamics along with the spatial and temporal evolution of the system from the early stage of the collisions to the final state interactions.

For studies of hadron physics at RHIC, the PHENIX experiment [ 1] demonstrates good capability for particle identification (PID) for both charged hadrons ( $\pi^\pm$ ,  $K^\pm$ ,  $p$ ,  $\bar{p}$ ,  $d$  and  $\bar{d}$ ) and neutral pions over a broad momentum range. The charged hadrons can be identified with time-of-flight measurements in two different detectors: (1) a high resolution Time-of-Flight wall (TOF) and, (2) an electro-magnetic calorimeter (EMC), in conjunction with the tracking system in the PHENIX central arm spectrometers and the beam counter, which provides the start timing and the event vertex determination. The tracking system in the central arm consists of drift chambers (DC), three layers of pad chambers (PC), and time expansion chambers (TEC). The PHENIX central arms cover  $|\eta| < 0.35$  in pseudo-rapidity, and cover  $\pi/4$  with the TOF and  $3\pi/4$  by EMC in azimuth. The  $\pi/K$  and  $K/p$  separation can be achieved up to 2 and 4 GeV/ $c$  in  $p_T$ , respectively, using the TOF detector, which has a 120 ps timing resolution. The EMC offers a larger azimuthal coverage for PID, but suffers from a timing resolution of only 500 ps. Neutral pions are identified with the EMC via the  $\pi^0 \rightarrow \gamma\gamma$  decay channel up to 10 GeV/ $c$  in  $p_T$  using the full statistics taken during Run II at RHIC in Au+Au collisions [ 2].

---

\*for the full PHENIX Collaboration author list and acknowledgements, see Appendix ‘‘Collaborations’’ of this volume.

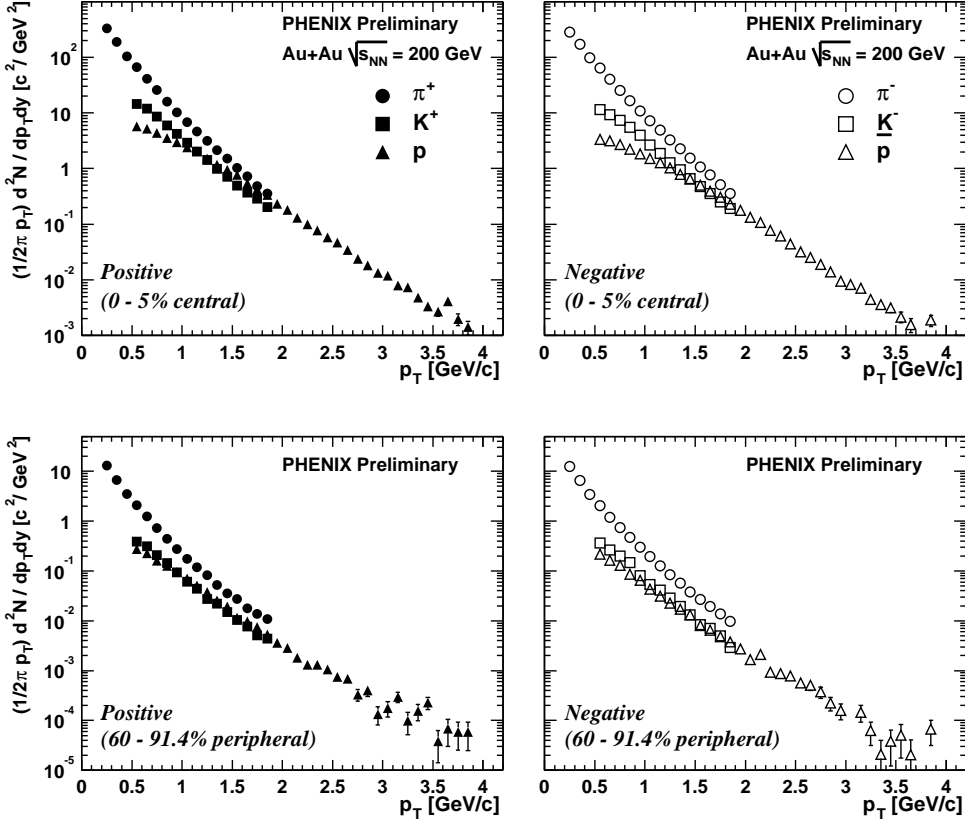


Figure 1. Transverse momentum distributions for pions (circles), kaons (squares) and  $p$ ,  $\bar{p}$  (triangles) in the 0–5% most central events (upper panels) and 60–91.4% most peripheral events (lower panels) at  $\sqrt{s_{NN}} = 200$  GeV in Au+Au collisions. The left panels show positive particles and the right panels show negative particles. The error bars are statistical only.

## 2. IDENTIFIED SINGLE PARTICLE SPECTRA

We have measured the transverse momentum distributions for  $\pi^\pm$ ,  $K^\pm$ ,  $p$  and  $\bar{p}$  at mid-rapidity in Au+Au collisions at  $\sqrt{s_{NN}} = 200$  GeV over a broad momentum range over various centrality selections. To identify the charged particles, the high resolution TOF counter is used in this analysis. We use about 4 million minimum bias events. The data are classified into 11 centrality bins expressed in percent of the total inelastic cross section. The spectra for each particle species are corrected for geometrical acceptance, decay in flight, multiple scattering, and tracking efficiency using a single particle Monte Carlo simulation. A multiplicity-dependent track reconstruction efficiency is also determined and applied by embedding simulated tracks into real events.

The upper two panels in Figure 1 show the  $p_T$  distributions for identified hadrons in the most central events (0–5%) in 200 GeV Au+Au collisions for positive (left) and negative

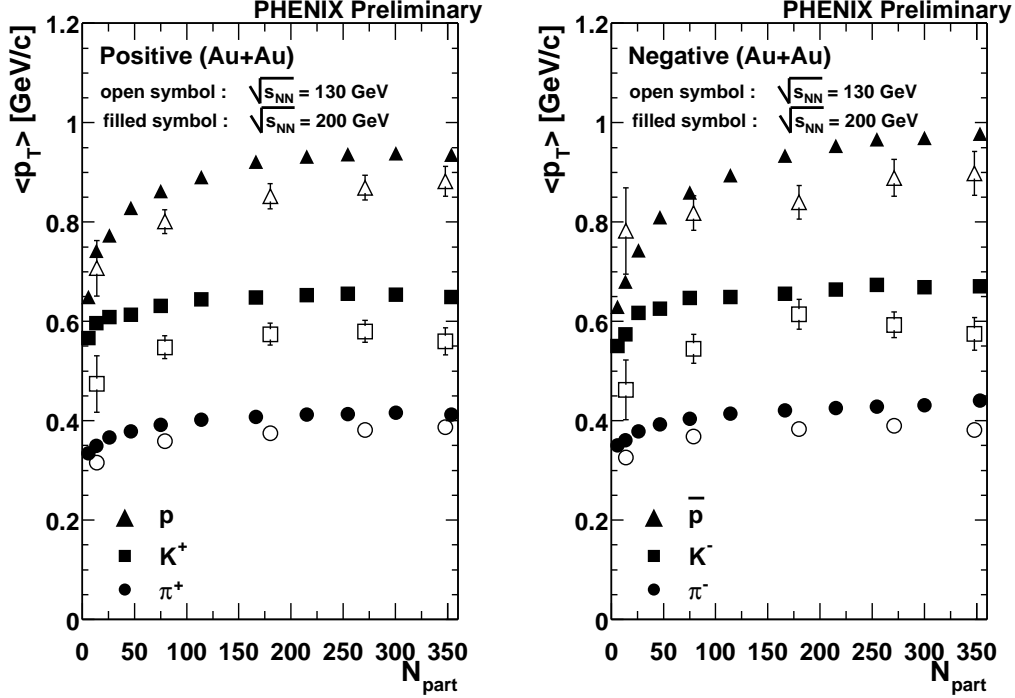


Figure 2. Mean transverse momentum for identified charged hadrons as a function of  $N_{part}$  for protons and anti-protons (triangles), kaons (squares) and pions (circles). The left panel shows positive particles and right panel shows negative particles. The open symbols indicate the data for 130 GeV [ 3] while the filled symbols indicate the data for 200 GeV in Au+Au collisions.

(right) particles. The lower two panels show the most peripheral events (60–91.4%). In each panel, the data are presented up to 1.8 GeV/c for charged pions and kaons, and 3.8 GeV/c for  $p$  and  $\bar{p}$ . In the low  $p_T$  region of the most central events, the data indicate that the inverse slope increases with the particle mass. Also, the shape of the  $p$  and  $\bar{p}$  spectra have a shoulder-arm shape while the pion spectra have a concave shape. On the other hand, in the most peripheral events, the spectra are almost parallel to each other. This mass dependence of the slopes and shapes of the spectra for protons in the central events can be explained by a radial flow picture. At around 2.0 GeV/c in central events, the proton yield becomes comparable to the pion yield. A similar behavior is also seen for negatively charged particles.

In order to quantify the observed mass dependence of the slopes, the mean transverse momenta  $\langle p_T \rangle$  are extracted for 11 centrality selections and for each particle species. The  $p_T$  spectra are extrapolated to below and above the measured range using a power law function for pions, an  $m_T$  exponential function for kaons, and a Boltzmann function for  $p$  and  $\bar{p}$ . In Figure 2, the centrality dependence of  $\langle p_T \rangle$  for identified charged hadrons are

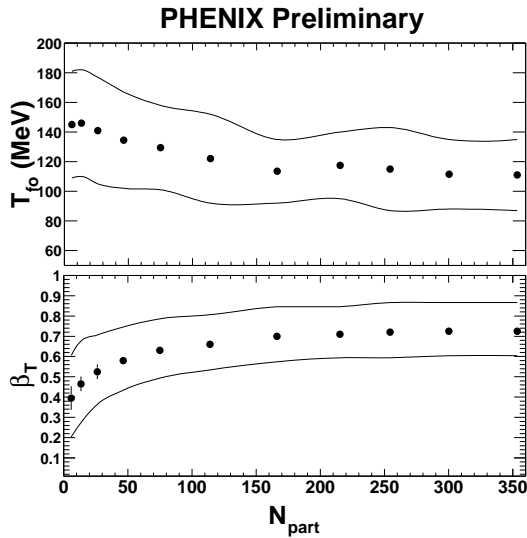


Figure 3. Freeze-out temperature (top) and transverse flow velocity (bottom), as a function of  $N_{part}$ , extracted from the hydrodynamical collective flow model fit to the single particle spectra at  $\sqrt{s_{NN}} = 200$  GeV in Au+Au.

shown together with the 130 GeV data points [ 3]. In both the 200 GeV and 130 GeV data,  $\langle p_T \rangle$  for all particle species increases from the most peripheral to the most central events and also increases with particle mass. The dependence of  $\langle p_T \rangle$  on particle mass suggests the existence of a collective hydrodynamical expansion. The dependence on the number of participant nucleons ( $N_{part}$ ) calculated using a Glauber model [ 4] may be due to an increasing radial expansion from peripheral to central events.

Using these  $p_T$  distributions, one can characterize the collision system with a small set of hydrodynamic quantities based on the expanding source model [ 6]: transverse flow velocity ( $\beta_T$ ) and freeze-out temperature ( $T_{fo}$ ). By using this model, which assumes boost invariance and a linear velocity profile, a simultaneous fit has been performed for the measured spectra in 200 GeV Au+Au in eleven different centrality selections [ 5]. For the 0–5% central events, an expansion flow velocity on the surface,  $\beta_T$ , of  $0.7 \pm 0.2$  (syst.) and a common freeze-out temperature,  $T_{fo}$ , of  $110 \pm 23$  (syst.) MeV is extracted. The fit results of all particles within each event centrality are shown in Figure 3. The top panel is for  $T_{fo}$  and the bottom panel is for  $\beta_T$ , both plotted as a function of  $N_{part}$ . Within the systematic uncertainties, the expansion parameters  $T_{fo}$  and  $\beta_T$  decrease and increase, respectively, with the number of participants, saturating at mid-centrality.

### 3. TWO-PARTICLE HBT CORRELATIONS

Another way to extract information about the particle emitting source created in relativistic heavy ion collisions is with two-particle HBT correlations. The HBT measurement is sensitive to the space-time evolution and duration time of the system at the freeze-out stage. Using the large data sample of pion pairs collected in Run II, we extend our HBT measurements up to 1.2 GeV/c in the transverse momentum of the pairs ( $k_T$ ) for pions [ 7]. In this analysis the Bertsch-Pratt parameterization is employed in a longitudinal co-moving system (LCMS), where the three-dimensional Gaussian radius parameters are  $R_{side}$ ,  $R_{out}$  and  $R_{long}$ . These radius parameters are studied as a function of  $k_T$  and centrality. We use 50 million minimum bias events with charged pions identified using the time-of-flight measurement in the EMC. A full Coulomb correction is applied assuming a

Gaussian source and no pairs coming from resonance decays.

As shown in reference [ 7], we have observed a clear  $k_T$  dependence for all Bertsch-Pratt radius parameters for pions in 200 GeV Au+Au collisions. This  $k_T$  dependence of the radius parameters can be explained by a space-momentum correlation effect due to the expansion of the system [ 8]. For the study of the duration time of the system, the ratio  $R_{out}/R_{side}$  can be used. In Figure 4, the ratio  $R_{out}/R_{side}$  as a function of  $k_T$  (left) and  $N_{part}$  for pion pairs is shown. The ratio does not change as a function of both  $k_T$  and centrality within the experimental uncertainties. In contrast to the success of the hydrodynamic model for  $p_T$  distributions in Section 2 of this paper, the HBT radii from the hydrodynamic calculation agree only qualitatively with the data with significant quantitative discrepancies [ 11]. At this time, no  $\chi^2$  minimum could be found for the simultaneous hydrodynamic fit of the particle spectra and the  $k_T$  dependence of HBT radius parameters for pions [ 5].

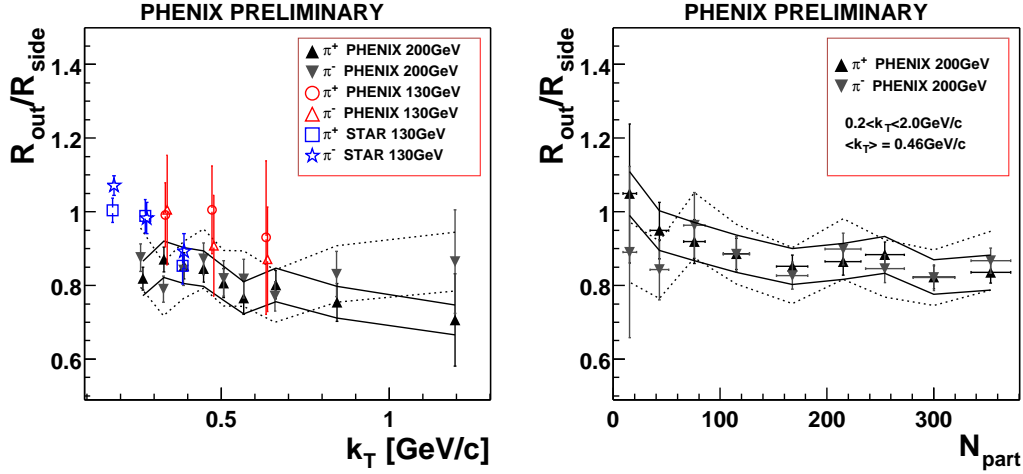


Figure 4. The ratio  $R_{out}/R_{side}$  for pions as a function of  $k_T$  (left) and  $N_{part}$  (right) with statistical error bars (200 GeV data only) and a systematic error band. In the left figure, results from PHENIX and STAR at 130 GeV are also shown [ 9, 10].

#### 4. DEUTERON AND ANTI-DEUTERON SPECTRUM

Deuteron and anti-deuteron measurements provide complementary information to the HBT measurements because the coalescence coefficient  $B_2$  [ 12] is considered to be proportional to the inverse of the volume of the system, and the dynamical evolution of the system can be studied with the  $p_T$  dependence of  $B_2$ , similar to two-particle HBT measurements.

Figure 5 shows the  $p_T$  distributions of  $d$  (squares) and  $\bar{d}$  (triangles) for minimum bias events in 200 GeV Au+Au collisions, identified with the high resolution TOF detector.

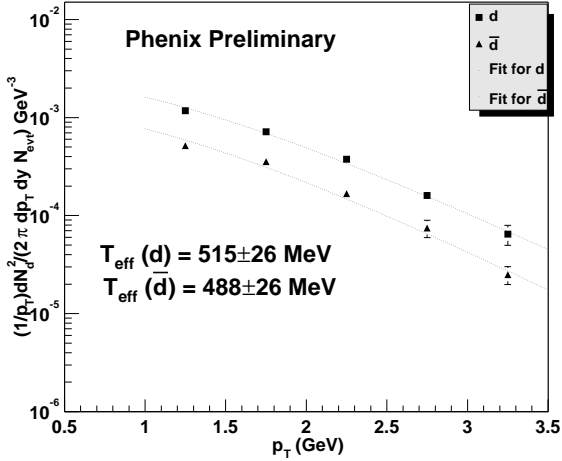


Figure 5.  $p_T$  distributions for deuterons (squares) and anti-deuterons (triangles). The error bars are statistical only. The lines are fits using an  $m_T$  exponential function.

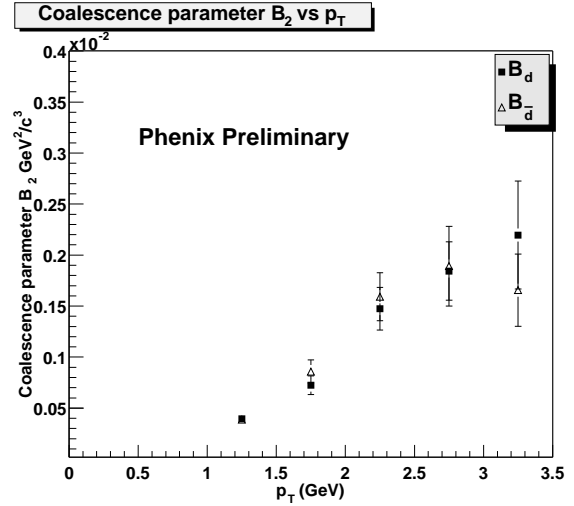


Figure 6.  $p_T$  dependence of the coalescence parameter,  $B_2$ , for deuterons (squares) and anti-deuterons (triangles) at mid-rapidity.

The fitted lines using an  $m_T$  exponential function are also shown. We obtain an effective temperature of  $515 \pm 26$  (stat.) MeV for deuterons and  $488 \pm 26$  (stat.) MeV for  $\bar{d}$ . Figure 6 shows the transverse momentum dependence of  $B_2$  for deuterons (square) and anti-deuterons (triangle) at mid-rapidity.  $B_2$  increases linearly with  $p_T$  up to 3.5 GeV/ $c$ . The  $p_T$  dependence of  $B_2$  is consistent with the expanding source picture. A similar behavior has been observed in the HBT radius parameters for pions [ 7].

## 5. PARTICLE RATIOS

Particle ratios provide us with information about the chemical properties of the collision system. In Figure 7, the particle ratios of  $\pi^-/\pi^+$  (left) and  $K^-/K^+$  (right) are shown as a function of  $p_T$  for central (0–5%) and peripheral (60–91.4%) Au+Au and proton-proton collisions at  $\sqrt{s_{NN}} = 200$  GeV. A similar plot for the  $\bar{p}/p$  ratio is shown in Figure 8 [ 13]. Regardless of the particle species, centrality, or collision system, the particle ratios are almost flat as a function of  $p_T$  within the systematic errors and measured  $p_T$  range, with the exception of the  $\bar{p}/p$  ratio for peripheral events, which seems to decrease in the high  $p_T$  region. The integrated ratios over the measured  $p_T$  range in the most central events in 200 GeV Au+Au collisions are:  $1.02 \pm 0.02$  (stat.)  $\pm 0.1$  (sys.) for  $\pi^-/\pi^+$ ,  $0.92 \pm 0.03$  (stat.)  $\pm 0.1$  (sys.) for  $K^-/K^+$ , and  $0.70 \pm 0.04$  (stat.)  $\pm 0.1$  (sys.) for  $\bar{p}/p$ . Based on a simple statistical thermal model [ 14], a baryon chemical potential,  $\mu_B$ , of  $\sim 30$  MeV for 200 GeV Au+Au central collisions is estimated from the  $K^-/K^+$  and  $\bar{p}/p$  ratios.

Particle composition at high  $p_T$  is also interesting in order to understand baryon production and transport, system evolution, and the interplay between soft processes and jet quenching in hard processes. In Figure 9, the  $p/\pi$  and  $\bar{p}/\pi$  ratios are shown. For

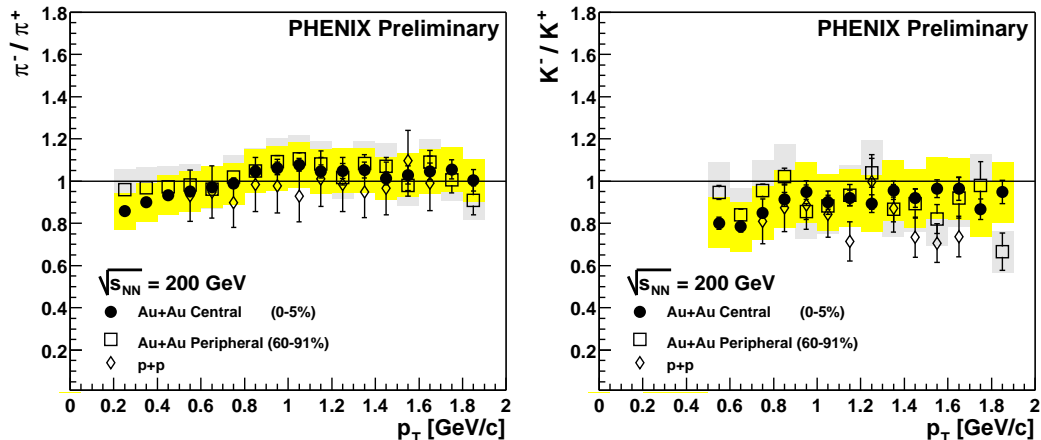


Figure 7. Particle ratios of  $\pi^-/\pi^+$  (left) and  $K^-/K^+$  (right) as a function of  $p_T$ . The data points are for the most central (filled circles) and the most peripheral (open squares) in Au+Au and proton-proton (open diamonds) collisions at  $\sqrt{s_{NN}} = 200$  GeV.

the denominator of the ratio  $p/\pi$  and  $\bar{p}/\pi$ , we use two independent measurements with different subsystems: (1)  $p_T$  spectra for  $\pi^\pm$  up to 2 GeV/c identified using the TOF, 2) neutral pions results from 1 GeV/c to 3.8 GeV/c measured using the EMC. Both the  $p/\pi$  and  $\bar{p}/\pi$  ratios have a clear centrality dependence. The data shows that these ratios in central collisions reach unity at a  $p_T$  of 2~3 GeV/c, while they saturate at around  $p_T$  of 0.3 – 0.4 in peripheral collisions. This observed behavior in central events may be attributed to the composition of two effects including a larger flow effect for protons (and  $\bar{p}$ ) compared to pions, and a pion suppression effect at high  $p_T$  [ 15].

## 6. ELLIPTIC FLOW FOR IDENTIFIED HADRONS

In non-central collisions, the initial overlap region of two nuclei is elliptically deformed in the transverse plane, resulting in anisotropic pressure gradients. These cause a more rapid expansion into the reaction plane than perpendicular to it, resulting in an anisotropy of the final  $p_T$  distributions called elliptic flow [ 11]. Since the event anisotropy is considered to be developed at the early stage of collisions, the study of elliptic flow provides a good tool to investigate the possible formation of a QGP state.

Elliptic flow is quantified by the second harmonic coefficient ( $v_2$ ) of a Fourier expansion in the azimuthal distributions of the measured spectrum with respect to the reaction plane. We have measured the  $v_2$  parameter for identified particles with respect to the reaction plane, which is defined in the beam counters ( $|\eta| = 3 \sim 4$ ) in 200 GeV Au+Au collisions. The details of the analysis method and results are shown in [ 16]. Figure 10 shows the  $p_T$  dependence of the  $v_2$  parameter for identified particles with respect to the reaction plane for minimum bias events. The solid circles are for protons and  $\bar{p}$ , and the

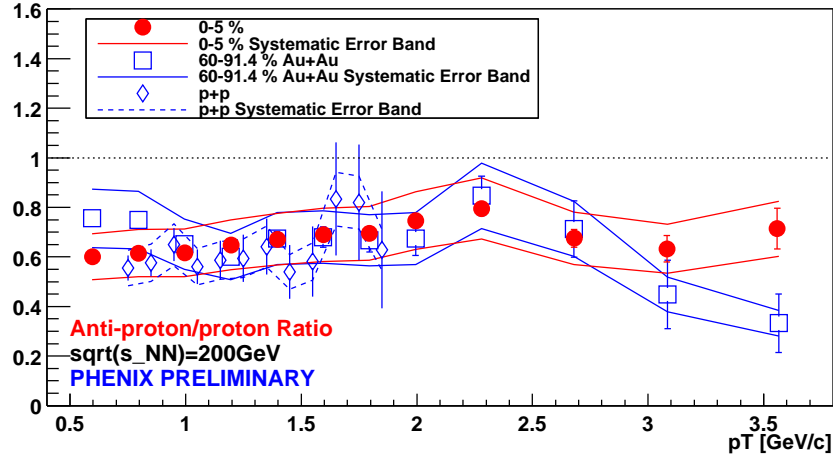


Figure 8.  $\bar{p}/p$  ratios as a function of  $p_T$  for central 0–5% (filled circles), peripheral 60–91.4% (open squares) Au+Au and proton-proton (open diamonds) collisions at  $\sqrt{s_{NN}} = 200$  GeV. The error bars indicate the statistical errors and the lines indicate the systematic errors for each data point.

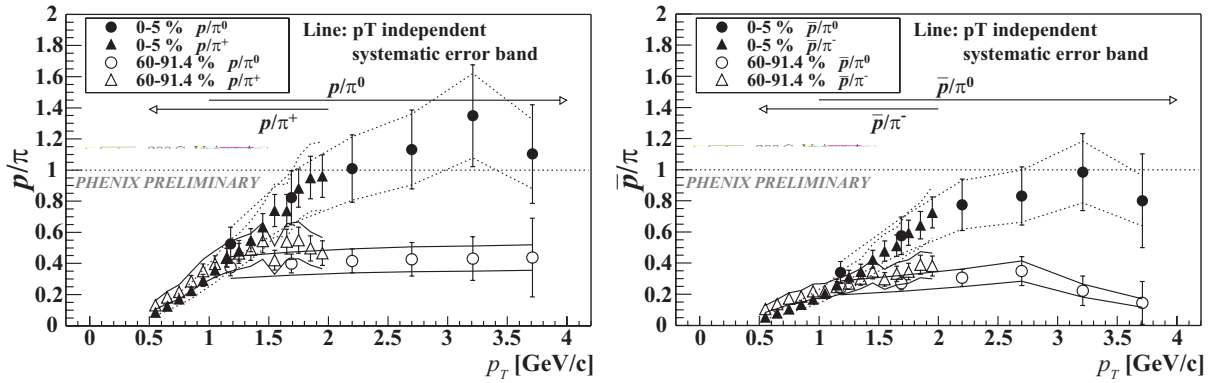


Figure 9.  $p/\pi$  (left) and  $\bar{p}/\pi$  (right) ratios as a function of  $p_T$  for the 0–5% and 60–91.4% centrality selections. Lines along the data points show the  $p_T$ -independent systematic error bands. The error bars show the statistical and  $p_T$ -dependent systematic errors, summed in quadrature.



open triangles are for the combined results for pions and kaons. The left panel shows negatively charged particles and the right panel shows positively charged particles. The solid lines are the results of a hydrodynamic calculation including a first order phase transition with a freeze-out temperature of 120 MeV [ 17]. The data shows that at lower  $p_T$  ( $< 2$  GeV/ $c$ ), the light mesons have a larger  $v_2$  parameter compared to protons and  $\bar{p}$ . The model calculation agrees very well with the data for all particles in this  $p_T$  range. However, the data seems to deviate from the hydrodynamic calculations above 2 GeV/ $c$  for mesons and baryons. In addition, the model cannot reproduce the opposite mass dependence of the  $v_2$  parameter, which is observed above 2 GeV/ $c$ .

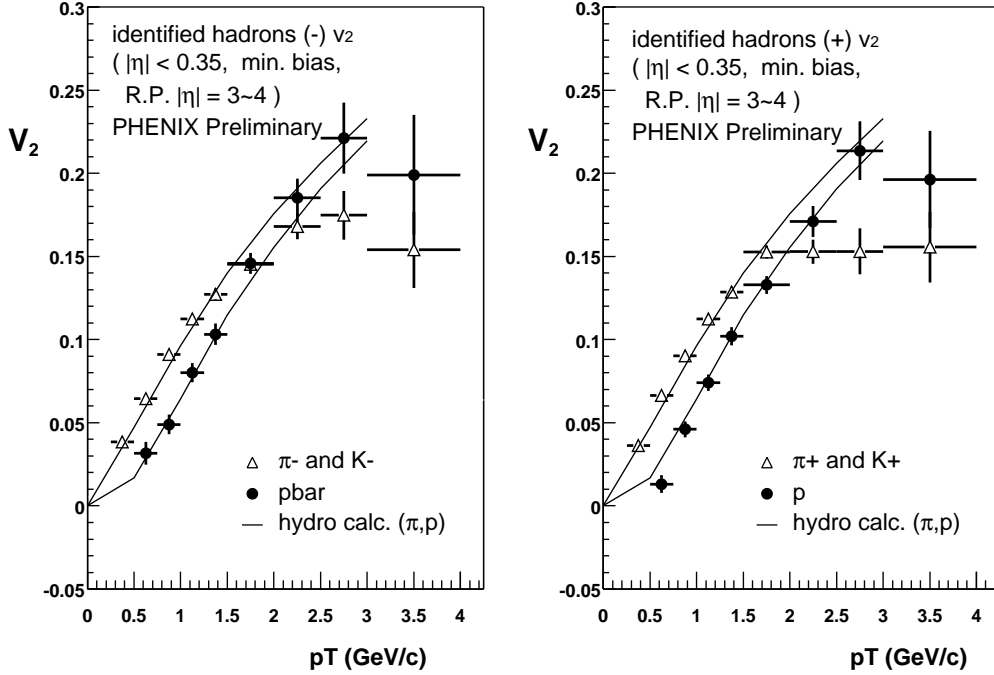


Figure 10. Transverse momentum dependence of  $v_2$  with respect to the reaction plane for  $(\pi^- + K^-)$  and  $\bar{p}$  (left), and for  $(\pi^+ + K^+)$  and  $p$  (right). The solid lines represent the hydrodynamic calculation [ 17] for pions (upper curve) and protons (lower curve).

## 7. SUMMARY

We present results on identified hadrons in Au+Au collisions at  $\sqrt{s_{NN}} = 200$  GeV at mid-rapidity over different centrality selections from the PHENIX experiment. The transverse momentum distributions for  $\pi^\pm$ ,  $K^\pm$ ,  $p$ ,  $\bar{p}$ ,  $d$ , and  $\bar{d}$  are measured and we observe a mass dependence of the slopes and shapes of the identified charged spectra in central

events. However, they are almost parallel to each other in the most peripheral events. Also, the mean transverse momentum for all particle species increases from peripheral to central events, and with particle mass. In two-particle HBT correlations for pions, there is a clear  $k_T$  dependence of all radius parameters. These results on the single particle spectra and two-particle HBT correlations are qualitatively consistent with a hydrodynamic collective expanding source picture, although there are quantitative discrepancies between the model and the HBT results. To characterize the collision system created in Au+Au collisions at RHIC energy, the flow velocity and freeze-out temperature have been extracted within the framework of a hydrodynamic expanding source model.

We also present results on the particle ratios  $\pi^-/\pi^+$ ,  $K^-/K^+$ , and  $\bar{p}/p$  as a function of  $p_T$  for different centralities in Au+Au and proton-proton collisions. It is found that the ratios are almost constant regardless of particle species, centrality, and collision system. The ratios  $p/\pi$  and  $\bar{p}/\pi$  up to 3.8 GeV/ $c$  are also measured by using the combined results for charged and neutral pions. In central collisions, the ratio reaches unity at a  $p_T$  of 2~3 GeV/ $c$  and saturates at a  $p_T$  around 0.3 – 0.4 GeV/ $c$  in peripheral collisions.

Finally, we present elliptic flow measurements with respect to the reaction plane for identified particles. The data show that at low  $p_T$  ( $< 2$  GeV/ $c$ ) the light mesons have a larger  $v_2$  parameter compared to protons and  $\bar{p}$ . The hydrodynamic model calculation agrees very well with the data for all particles up to 2 GeV/ $c$ . However, the data seems to deviate from the hydrodynamic model above 2 GeV/ $c$  for both mesons and baryons. The model cannot reproduce the opposite mass dependence of the  $v_2$  parameter above 2 GeV/ $c$ .

## REFERENCES

1. PHENIX Collaboration, Nucl. Inst. to be submitted.
2. D. G. D'Enterria, for the PHENIX Collaboration, these proceedings.
3. K. Adcox et al., Phys. Rev. Lett. **88**, 242301 (2002).
4. K. Adcox et al., Phys. Rev. Lett. **86**, 3500 (2002).
5. J. Burward-Hoy, for the PHENIX Collaboration, these proceedings.
6. Schnedermann, Sollfrank and Heinz, Phys. Rev. C **48**, 2462 (1993).
7. A. Enokizono, for the PHENIX Collaboration, these proceedings.
8. Y. F. Wu et al., Eur. Phys. J. C **1**, 599 (1998).
9. K. Adcox et al., Phys. Rev. Lett. **88**, 192302 (2002).
10. C. Adler et al., Phys. Rev. Lett. **87**, 082301 (2001).
11. U. Heinz and P. F. Kolb, hep-ph/0204061.
12. S. T. Butler and C. A. Pearson, Phys. Rev. **129**, 836 (1963).
13. T. Sakaguchi, for the PHENIX Collaboration, these proceedings.
14. F. Becattini et al., hep-ph/0002267.
15. K. Adcox et al., Phys. Rev. Lett. **88**:022301, (2002).
16. S. Esumi, for the PHENIX Collaboration, these proceedings.
17. P.Huovinen, P.F.Kolb, U.W.Heinz, P.V.Ruuskanen and S.A.Voloshin, Phys. Lett. B **503**, 58 (2001).